

LETTERS

# Magnetically and electrically polarization-tunable THz emitter with integrated ferromagnetic heterostructure and large-birefringence liquid crystal

To cite this article: Hongsong Qiu *et al* 2018 *Appl. Phys. Express* **11** 092101

View the [article online](#) for updates and enhancements.

## Related content

- [Electrically tunable terahertz polarization converter based on overcoupled metal-isolator-metal metamaterials infiltrated with liquid crystals](#)  
Borislav Vasi, Dimitrios C Zografopoulos, Goran Isi *et al*.
- [Bursts of efficient terahertz radiation with saturation effect from metal-based ferromagnetic heterostructures](#)  
Shunnong Zhang, Zuanming Jin, Zhendong Zhu *et al*.
- [Systematic experimental study on a highly efficient terahertz source based on two-color laser-induced air plasma](#)  
Jun Xie, Wen-Hui Fan and Xu Chen



## Magnetically and electrically polarization-tunable THz emitter with integrated ferromagnetic heterostructure and large-birefringence liquid crystal

Hongsong Qiu<sup>1</sup>, Lei Wang<sup>2</sup>, Zhixiong Shen<sup>3</sup>, Kosaku Kato<sup>1</sup>, Nobuhiko Sarukura<sup>1</sup>, Masashi Yoshimura<sup>1</sup>, Wei Hu<sup>3</sup>, Yanqing Lu<sup>3</sup>, and Makoto Nakajima<sup>1\*</sup>

<sup>1</sup>Institute of Laser Engineering, Osaka University, Suita, Osaka 5650871, Japan

<sup>2</sup>College of Electronic and Optical Engineering and College of Microelectronics, Nanjing University of Posts and Telecommunications, Nanjing 210023, China

<sup>3</sup>National Laboratory of Solid State Microstructures, Collaborative Innovation Center of Advanced Microstructures and College of Engineering and Applied Sciences, Nanjing University, Nanjing 210093, China

\*E-mail: nakajima-m@ile.osaka-u.ac.jp

Received June 14, 2018; accepted July 18, 2018; published online August 2, 2018

A magnetically and electrically polarization-tunable terahertz emitter that integrates a ferromagnetic heterostructure and large-birefringence liquid crystals is demonstrated. The heterostructure and the liquid crystal cell act as the broadband terahertz source and the phase retarder, respectively. The polarization state is switched between linear and circular by changing the direction of the external magnetic field. The phase retardation for frequencies higher than 1 THz is continuously adjustable over a range of  $\pi/2$  by applying a low voltage. This compact, broadband, economical, and easy-to-regulate terahertz emitter can be widely used in polarization-sensitive research and engineering applications.

© 2018 The Japan Society of Applied Physics

The past decades have seen great developments in the generation and applications of terahertz (THz) radiation.<sup>1–16</sup> Its polarization information provides deeper insights in various applications such as helical biopolymer sensing,<sup>14</sup> high-resolution topographic detection,<sup>15,16</sup> and research on spin dynamics.<sup>2–8</sup> Therefore, a broadband polarization-tunable THz emitter will be potentially useful in modern THz systems. One possible way to tune the polarization state of the THz wave is to modulate the phase retardation or azimuthal angle of the pump beams.<sup>17–20</sup> Another approach is inserting an additional wave plate in the linearly polarized THz system.<sup>21–23</sup> However, both methods are subject to complex adjustments to achieve control of the polarization state in a broad THz region, making it inconvenient in practical applications.

A new THz emitter based on spin currents in the ferromagnetic heterostructure has been proposed in recent years.<sup>1,24–26</sup> The compact heterostructure emitter covers a frequency range of around 30 THz. The polarization of the THz wave, which is perpendicular to the spin polarization, can be conveniently controlled in a contactless manner by applying an external magnetic field. Nevertheless, its polarization tunability is only limited to the direction change of the linear THz wave. To date, the lack of a broadband and easy-to-regulate THz source with comprehensive polarization tunability significantly restricts the development of polarization-sensitive applications.

Liquid crystals (LCs) have attracted wide interest as continuously variable retarders owing to their relatively large birefringence in a wide frequency range and easy-to-modulate properties.<sup>27–31</sup> Wang et al. developed the electrically tunable broadband THz wave plates by using the large-birefringence LC NJU-LDn-4.<sup>29,30</sup> Moreover, given the advantages of flexibility and compact cell structure of the LC THz wave plate, it can be mounted on a broadband THz emitter to make it an integral THz active device. The ferromagnetic heterostructure would be a promising choice for this purpose. Both the heterostructure emitter and the LC wave plate have the characteristics of compact structure and broad band. Furthermore, the metallic layers of the emitter can be reused as a ready-made electrode in the LC cells. The compact assembly

of a LC wave plate and ferromagnetic heterostructure can provide THz waves with various polarization states. To the best of our knowledge, similar highly integrated tunable THz emitters have never been reported.

In this article, we demonstrate a magnetically and electrically polarization-tunable THz emitter in which a ferromagnetic heterostructure and a large-birefringence LC cell are integrated. The phase retardation and the state of polarization can be conveniently controlled by adjusting the externally applied electric field and magnetic field, respectively. This conveniently controlled THz emitter will provide more effective solutions in polarization-related applications.

Figure 1(a) schematically illustrates the structure of the integrated THz emitter Co/Pt/LC. It contains a ferromagnetic heterostructure, large-birefringence LC cell, and few-layer porous graphene electrode. In our experiments, a 10-nm-thick cobalt (Co) layer and a 7-nm-thick platinum (Pt) layer were deposited on the front fused-silica substrate (0.5 mm thick) as the ferromagnetic (FM) and nonmagnetic (NM) layers, respectively. The substrates were cleaned using acetone and isopropyl alcohol in the ultrasonic machine in advance to remove any contamination. Both layers were grown by electron beam evaporation under ultrahigh vacuum at room temperature. The rear substrate was covered with porous few-layer graphene. The graphene was grown by CVD and transferred onto the rear fused-silica substrate (0.8 mm thick) with an improved transfer process, as described in the literature.<sup>32</sup> Porous structures were introduced onto the graphene films by operating UV/ozone treatment, giving rise to a transmittance as high as 98% in the THz region. Subsequently, sulfonic azo dye (SD1) was spin coated and photoaligned as the alignment layer material above the Pt and graphene layers. The SD1 layers ensure the homogeneous prealignment of the LC molecules. Two substrates were then stacked with 250- $\mu$ m-thick Mylar films between them to form a cell with uniform thickness. The cell was infiltrated with NJU-LDn-4 LC and sealed with epoxy glue. The alignment of the LC molecules (the director) was parallel to the direction that is  $-45^\circ$  to the  $x$ -axis in the  $x$ - $y$  plane. The directions parallel and perpendicular to the director are denoted as extraordinary ( $e$ ) and ordinary ( $o$ ) directions, respectively, as shown in Fig. 1(a).

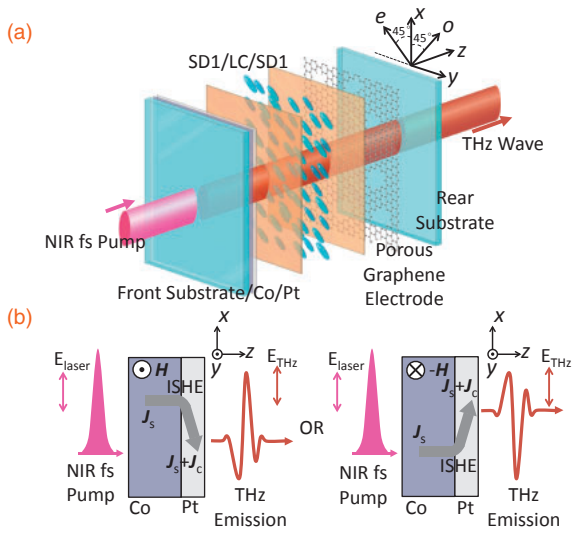


**Fig. 1.** Schematic of the polarization-tunable THz emitter. (a) A ferromagnetic heterostructure and a large-birefringence LC are integrated in the emitter. The heterostructure acts as the THz source as well as the electrode on the front side. A few-layer porous graphene with a high transmittance is employed as the other electrode on the rear side. (b) The spin current  $J_s$  launched by the laser pulse excitation is converted into the in-plane charge current  $J_c$  due to the ISHE. The current  $J_c$  along the  $x$ -axis acts as an electric dipole, emitting linearly polarized THz waves into free space. The polarity of the THz waveform is determined by the direction of the magnetic field  $H$  and reverses together with it.

The NJU-LDn-4 LC has a large birefringence in the THz region. The average birefringence of 0.306 in the range from 0.4 to 1.6 THz is obtained with a maximum of 0.314 at  $\sim 1.6$  THz.<sup>28)</sup> There is no sharp absorption in the frequency range investigated.

Figure 1(b) illustrates the mechanism of the linear THz emission from the Co/Pt layers. The Fermi-level electrons in the Co layer are excited to higher energy bands by ultrafast laser pulses within a few hundred femtoseconds. The photo-excited majority- and minority-spin electrons are mainly located in  $sp$  and  $d$  bands, respectively. The majority-spin electrons in  $sp$  bands have higher velocities than the minority-spin ones in  $d$  bands.<sup>33)</sup> As a result, the photocurrent in the Co layer is spin polarized, which is the so-called spin current. When the spin current  $J_s$  flows into the Pt layer, it is converted into the charge current  $J_c$  owing to the inverse spin Hall effect (ISHE).<sup>34)</sup> The transformation between the spin current and the charge current is described by  $J_c \propto \gamma J_s \times H$ , where  $\gamma$  is the spin Hall angle and  $H$  is the external magnetic field. The charge current  $J_c$  along the  $x$ -axis acts as an electric dipole, causing a linear THz emission  $E_{THz}$  to the free space. Because the direction of  $J_c$  is always perpendicular to that of  $H$ , the polarization of  $E_{THz}$  can be conveniently controlled by changing the direction of  $H$ . The linearly polarized THz wave can be decomposed into  $e$  and  $o$  components. The  $e$  component of the THz wave experiences a phase retardation relative to the  $o$  component. The phase retardation between them in a LC cell with the thickness of  $d$  is given by the equation  $\Delta\varphi = 2\pi(n_e - n_o)d/\lambda$ , where  $\lambda$  is the wavelength of the THz waves and  $n_e$  and  $n_o$  are the refractive indexes of the  $e$  and  $o$  waves, respectively.

The THz emitter was pumped by linearly polarized laser pulses under a normal incidence scheme with 100 fs duration, 1 kHz repetition rate, and 800 nm center wavelength from a

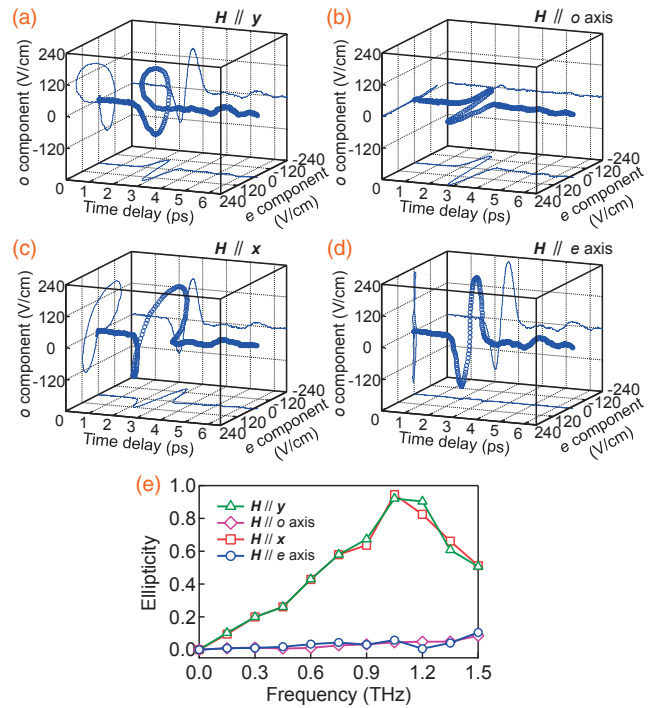


**Fig. 2.** Magnetic control of the polarization state. The magnetic field is applied along the (a)  $y$ -, (b)  $o$ -, (c)  $x$ -, and (d)  $e$ -axes. The state of the polarization of the emitted THz wave sequentially varies from (a) right circularly polarized light to (b) linearly polarized light along the  $e$ -axis, (c) left circular light, and (d) linearly polarized light along the  $o$ -axis. (e) Ellipticity spectra of the waveforms are shown in (a)–(d).

Ti:sapphire amplified laser. The diameter of the laser spot was 8 mm. The THz emission was collected and focused by three parabolic mirrors. The focused THz pulses are probed by electrooptic (EO) sampling using a 1-mm-thick (110)-oriented ZnTe crystal. During the experiment, the samples were kept in the saturated magnetization state by applying an external static magnetic field  $H$  ( $\sim 150$  mT). To measure the  $e$  and  $o$  components of the THz waveform independently, two wire grid polarizers were used. The transmission axis of the front polarizer was aligned along the  $e$ - or  $o$ -axis to separate these two components from each other. The transmission axis of the back polarizer was always aligned along  $x$ . The energy of each laser pulse is 0.15 mJ in all the measurements. The amplitude of the THz emission is on the order of 100 V/cm. It is around one order smaller than the emission amplitude of the 0.5-mm-thick (110)-oriented ZnTe crystal, which was measured in the same setup. The attenuation of the amplitude of the THz radiation after integrating the LC cell is less than 30%.

To study the effect of the external magnetic field on the state of the polarization of the THz emission, we applied  $H$  in various directions when no voltage was applied. Figures 2(a)–2(d) show the THz waveforms detected when  $H$  was along the  $y$ -,  $o$ -,  $x$ -, and  $e$ -axes, respectively. The coordinates are shown in Fig. 1(a). The external magnetic field controls the magnetization direction of the Co layer, which in turn changes the relative angle between the initial THz emission and the director of the LC cell. When  $H$  is applied in the  $y$ -direction, the THz wave from Co/Pt is polarized along  $x$  in accordance with the ISHE. There is a phase retardation for the  $e$  component relative to the  $o$  component and a right circularly polarized THz pulse is obtained from Co/Pt/LC. In contrast to that, when  $H$  is applied along the  $o$ -axis, the polarization of

the THz emission from Co/Pt is parallel to the  $e$ -axis of the LC, which gives rise to a retarded linearly polarized  $e$  wave from Co/Pt/LC. Analogously, we can also obtain a left circularly polarized pulse and a linearly polarized pulse by applying  $\mathbf{H}$  along the  $x$ - and  $e$ -axes. The state of the polarization alternates between linear and circular with each rotation of  $\mathbf{H}$  around the  $z$ -axis by  $45^\circ$ . Figure 2(e) shows the ellipticity spectra of the THz waves shown in Figs. 2(a)–2(d). An almost perfect circular wave can be achieved at 1 THz when the magnetic field is applied along  $x$  and  $y$ . For frequencies higher and lower than 1 THz, the waves are elliptically polarized.

Next, we discuss the electrical responses of the Co/Pt/LC emitter when the magnetic field is kept along  $y$ . The metallic layer also acts as the front electrode, paired with the graphene layers on the rear, to generate a uniform electric field in the LC cell. The cells were driven by a 1 kHz square-wave alternating voltage source. When the voltage is applied across the LC cell, the molecules tend to align along the electric field. The director rotates from the in-plane to out-of-plane direction continuously with increasing voltage, so that there will be no phase difference between the  $e$  and  $o$  waves when it reaches the saturation voltage. Figure 3(a) demonstrates the electrical modulation of the phase retardations between the  $o$  and  $e$  components. The  $o$  wave leads the  $e$  wave by  $\sim 0.21$  ps without voltage. When a voltage is applied, the  $o$  wave does not show a clear change, while the  $e$  waves shift toward the  $o$  wave in the time domain. The phase retardation vanishes when the voltage is above 8 V. Figure 3(b) reveals the frequency-dependent phase retardation under various voltages. A linear relationship between the phase retardation and the frequency can be seen clearly because of the low dispersion of the LC over a broadband range. Phase retardation larger than  $\pi/2$  can be achieved when the frequency is above 1 THz. By applying an appropriate voltage, a wave with arbitrary ellipticity can be obtained in the frequency range from 1 to 1.5 THz. Consistent with the results shown in Fig. 3(a), there is almost no phase difference throughout the entire frequency range in Fig. 3(b) when the saturation voltage of around 8 V is applied. It is worth noting that we observed higher sensitivity in the electrical control of the LC than the results reported in the previous work, in which the voltage of  $\sim 20$  V was required.<sup>29)</sup> The LC material (NJU-LDn-4 LC) and the thickness of the LC cell (250  $\mu\text{m}$ ) were identical in these two works. The rear electrodes (porous few-layer graphene) in both works were fabricated and transferred in the same way. However, in the earlier work, a metal wire grid,<sup>29)</sup> instead of the metallic layer, was used as the front electrode. Compared with the wire grid electrode, the fully covered electrode on the entire surface in this work provides a stronger and more homogenous electric field under the same voltage, subsequently giving rise to a higher modulating sensitivity.

The ellipticity evolutions with the operating voltage at 1 and 1.5 THz are shown in Fig. 3(c). The ellipticity sensitively depends on the operating voltage and tends to become zero when a high operating voltage is applied. A nearly circularly polarized wave is obtained at 1 THz without applying voltage. In contrast, an operating voltage of around 1.3 V is necessary to obtain a circularly polarized wave at 1.5 THz. This value is estimated by fitting and extrapolation. It means that even though the circular polarization is only realized in a limited

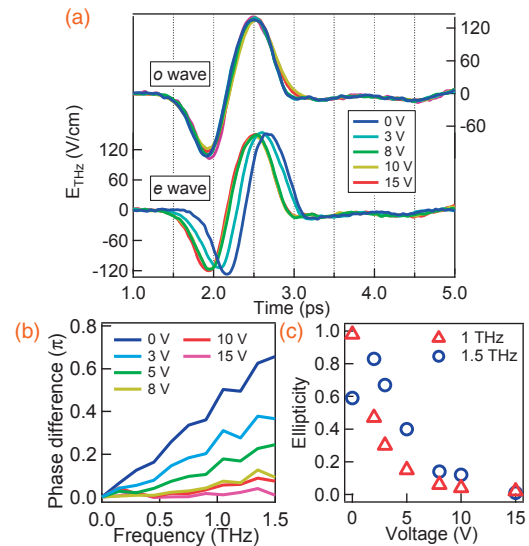


**Fig. 3.** Electric modulation of the phase retardation. (a) The phase retardation between the  $o$  and  $e$  light becomes smaller with the application of a voltage between the metallic layer electrode and the graphene electrode. The phase retardation vanishes when the voltage is around 8 V. (b) Frequency dependence of phase difference with the application of various voltages. (c) Relationship between voltage and ellipticity at 1 and 1.5 THz.

bandwidth, we can tune the frequency range by applying an appropriate operating voltage. In our experiments, the minimum value of the tunable frequency is 1 THz on account of the small thickness of the LC. If we use a thicker LC cell, for example, a double-stacked LC cell, we can extend the tunable range to a lower frequency range.<sup>29)</sup> Furthermore, the small deviation of the ellipticity with regard to 1 at 0 V is mainly due to the difference between the losses along the  $e$ - and  $o$ -axes in the LC cell. The amplitudes of the two components are slightly different. One possible solution can be to compensate the amplitude difference by changing the direction of the external magnetic field  $\mathbf{H}$  precisely. Given the thickness of the LC cell in our device, the electric response time is on the scale of seconds. In contrast, the magnetic response time is determined by the magnetization process of the Co layer, which is around 10 ns.<sup>35)</sup> Our polarization-tunable THz source in the broadband can be used as a powerful tool in the sensing of polarization-sensitive samples, e.g., the helical biological molecule. In addition, in engineering applications, the compact and economical polarization-tunable THz source can also be implemented in mechanical processing machines to operate in situ topographic measurements on surface samples.

In summary, we demonstrate a magnetically and electrically polarization-tunable THz emitter in which a ferromagnetic heterostructure and a large-birefringence liquid crystal cell are integrated. The ferromagnetic heterostructure acts as the THz source as well as the electrode on the optical pumping side. A few-layer porous graphene with a high transmittance is employed as the other electrode on the rear side. The state of the polarization can be switched between linear and circular in a noncontact manner by changing the direction of the external magnetic field. The phase retardation between  $e$  and  $o$  waves can be electrically tuned with a high efficiency. This compact and economical THz emitter can be widely used for polarization-sensitive research and engineering applications.

**Acknowledgments** This work was supported by the Japan Society for the Promotion of Science (JSPS), KAKENHI (JP16H03886, JP18H04515); NEDO of the Ministry of Economy, Trade, and Industry of Japan (METI); National Natural Science Foundation of China (NSFC) (61605088); and Natural Science Foundation of Jiangsu Province (BK20150845). The fabrication of the Co/Pt heterostructures in this work was supported by the “Nanotechnology Platform Project in Osaka University” of the Ministry of Education, Culture, Sports, Science and Technology, Japan (F-18-OS-0003, S-18-OS-0003).

- 1) T. Kampfrath, M. Battiato, P. Maldonado, G. Eilers, J. Nötzold, S. Mährlein, V. Zbarsky, F. Freimuth, Y. Mokrousov, S. Blügel, M. Wolf, I. Radu, P. M. Oppeneer, and M. Münzenberg, *Nat. Nanotechnol.* **8**, 256 (2013).
- 2) A. Namai, M. Yoshikiyo, K. Yamada, S. Sakurai, T. Goto, T. Yoshida, T. Miyazaki, M. Nakajima, T. Suemoto, H. Tokoro, and S. Ohkoshi, *Nat. Commun.* **3**, 1035 (2012).
- 3) M. Nakajima, A. Namai, S. Ohkoshi, and T. Suemoto, *Opt. Express* **18**, 18260 (2010).
- 4) K. Yamaguchi, M. Nakajima, and T. Suemoto, *Phys. Rev. Lett.* **105**, 237201 (2010).
- 5) K. Yamaguchi, T. Kurihara, Y. Minami, M. Nakajima, and T. Suemoto, *Phys. Rev. Lett.* **110**, 137204 (2013).
- 6) T. Kurihara, H. Watanabe, M. Nakajima, S. Karube, K. Oto, Y. C. Otani, and T. Suemoto, *Phys. Rev. Lett.* **120**, 107202 (2018).
- 7) M. Nakajima, T. Kurihara, Y. Tadokoro, B. Kang, K. Takano, K. Yamaguchi, H. Watanabe, K. Oto, T. Suemoto, and M. Hangyo, *J. Infrared Millimeter Terahertz Waves* **37**, 1199 (2016).
- 8) T. Kurihara, K. Nakamura, K. Yamaguchi, Y. Sekine, Y. Saito, M. Nakajima, K. Oto, H. Watanabe, and T. Suemoto, *Phys. Rev. B* **90**, 144408 (2014).
- 9) S. D. Ganichev and W. Prettl, *J. Phys.: Condens. Matter* **15**, R935 (2003).
- 10) Y. Minami, T. Kurihara, K. Yamaguchi, M. Nakajima, and T. Suemoto, *Appl. Phys. Lett.* **102**, 151106 (2013).
- 11) Y. Minami, M. Nakajima, and T. Suemoto, *Phys. Rev. A* **83**, 023828 (2011).
- 12) T. Matsui, H. Mori, Y. Inose, S. Kuromiya, K. Takano, M. Nakajima, and M. Hangyo, *Jpn. J. Appl. Phys.* **55**, 03DC12 (2016).
- 13) H. Qiu, T. Kurihara, H. Harada, K. Kato, K. Takano, T. Suemoto, M. Tani, N. Sarukura, M. Yoshimura, and M. Nakajima, *Opt. Lett.* **43**, 1658 (2018).
- 14) J. Xu, G. J. Ramian, J. F. Galan, P. G. Savvidis, A. M. Scopatz, R. R. Birge, S. J. Allen, and K. W. Plaxco, *Astrobiology* **3**, 489 (2003).
- 15) M. Okano and S. Watanabe, *Sci. Rep.* **6**, 39079 (2016).
- 16) N. Yasumatsu and S. Watanabe, *Opt. Lett.* **37**, 2706 (2012).
- 17) M. Li, H. Pan, Y. Tong, C. Chen, Y. Shi, J. Wu, and H. Zeng, *Opt. Lett.* **36**, 3633 (2011).
- 18) H. Wen and A. M. Lindenberg, *Phys. Rev. Lett.* **103**, 023902 (2009).
- 19) Q. Chen and X.-C. Zhang, *Appl. Phys. Lett.* **74**, 3435 (1999).
- 20) M. Sato, T. Higuchi, N. Kanda, K. Konishi, K. Yoshioka, T. Suzuki, K. Misawa, and M. Kuwata-Gonokami, *Nat. Photonics* **7**, 724 (2013).
- 21) A. C. Strikwerda, K. Fan, H. Tao, D. V. Pilon, X. Zhang, and R. D. Averitt, *Opt. Express* **17**, 136 (2009).
- 22) J. Masson and G. Gallot, *Opt. Lett.* **31**, 265 (2006).
- 23) Y. Kawada, T. Yasuda, A. Nakanishi, K. Akiyama, K. Hakamata, and H. Takahashi, *Opt. Lett.* **39**, 2794 (2014).
- 24) T. Seifert, S. Jaiswal, U. Martens, J. Hannegan, L. Braun, P. Maldonado, F. Freimuth, A. Kronenberg, J. Henrizi, I. Radu, E. Beaurepaire, Y. Mokrousov, P. M. Oppeneer, M. Jourdan, G. Jakob, D. Turchinovich, L. M. Hayden, M. Wolf, M. Münzenberg, M. Kläui, and T. Kampfrath, *Nat. Photonics* **10**, 483 (2016).
- 25) G. Torosyan, S. Keller, L. Scheuer, R. Beigang, and E. T. Pappaioannou, *Sci. Rep.* **8**, 1311 (2018).
- 26) H. S. Qiu, K. Kato, K. Hirota, N. Sarukura, M. Yoshimura, and M. Nakajima, *Opt. Express* **26**, 15247 (2018).
- 27) L. Wang, S. Ge, W. Hu, M. Nakajima, and Y. Lu, *Opt. Express* **25**, 23873 (2017).
- 28) L. Wang, X. Lin, X. Liang, J. Wu, W. Hu, Z. Zheng, B. Jin, Y. Qin, and Y. Lu, *Opt. Mater. Express* **2**, 1314 (2012).
- 29) L. Wang, X.-W. Lin, W. Hu, G.-H. Shao, P. Chen, L.-J. Liang, B.-B. Jin, P.-H. Wu, H. Qian, Y.-N. Lu, X. Liang, Z.-G. Zheng, and Y.-Q. Lu, *Light: Sci. Appl.* **4**, e253 (2015).
- 30) L. Wang, S. Ge, W. Hu, M. Nakajima, and Y. Lu, *Opt. Mater. Express* **7**, 2023 (2017).
- 31) C.-F. Hsieh, R.-P. Pan, T.-T. Tang, H.-L. Chen, and C.-L. Pan, *Opt. Lett.* **31**, 1112 (2006).
- 32) X. Li, Y. Zhu, W. Cai, M. Borysiak, B. Han, D. Chen, R. D. Piner, L. Colombo, and R. S. Ruoff, *Nano Lett.* **9**, 4359 (2009).
- 33) R. Knorren, K. H. Bennemann, R. Burgermeister, and M. Aeschlimann, *Phys. Rev. B* **61**, 9427 (2000).
- 34) E. Saitoh, M. Ueda, H. Miyajima, and G. Tatara, *Appl. Phys. Lett.* **88**, 182509 (2006).
- 35) J.-M. L. Beaujour, W. Chen, A. D. Kent, and J. Z. Sun, *J. Appl. Phys.* **99**, 08N503 (2006).